ACS OMEGA

Article

Cite This: ACS Omega 2019, 4, 19177−19182

http://pubs.acs.org/journal/acsodf

Effect of Molecular Structures of Donor Monomers of Polymers on Photovoltaic Properties

Ruiping Qin,*[,†,‡] Deen Guo,[‡] Heng Ma,[‡] Jien Yang,[†,‡] Yurong Jiang,[‡] Hairui Liu,[†,‡] Zhiyong Liu,[‡] Jian Song,[§] and ChaoChao Qin*[,§]

[†]Key Laboratory of Photovoltaic Materials of Henan Province, School of Material Science and Engineering, [‡]Key Laboratory of Photovoltaic Materials of Henan Province, School of Physics, and [§]School of Physics, Henan Normal University, Xinxiang 453007, China

Supporting Information

ABSTRACT: This work investigates the photovoltaic properties of polymers that include different carbazole blocks as electron donors (D) but the same benzothiadiazole derivative as the electron acceptor (A). Five D−A copolymers are studied with ultrafast intramolecular exciton splitting and recombination dynamics to acquire the single-molecule structure and their photovoltaic performance relationship. The photovoltaic parameters such as energy level, optical band gap, and light-harvesting ability are highly dependent on the molecular structure of the donor monomer (including their appended flexible alkyl chain). Branched or linear alkyl groups on the same D block obviously vary the polymer steady-state absorption spectra and film morphology. For organic solar cells, this work allows tuning and control of the ultrafast dynamics, implying photovoltaic material design in the future.

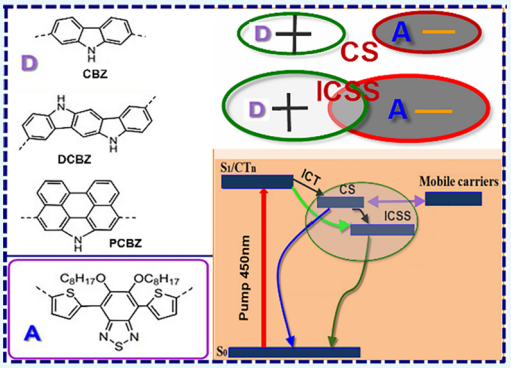

INTRODUCTION

World clean energy imperious demands inevitably trigger the rapid development of renewable energy technology.[1] Among these, solar power is the most abundant clean energy.[2,3] One of the direct applications of solar power is organic solar cells (OSCs).[4] Basically, OSCs' active layer was constructed by two types of organic semiconductors. One is a p-type electron donor, and the other is an n-type electron acceptor. The electronic nature of these different types of materials plenarily decides the device power conversion efficiency and application life span.[5] Hitherto, new materials and device engineering have pushed this technology to a great level which is already near the commercial application threshold.[6−8] All kinds of π-conjugated n- or p-type polymers because of their unique optoelectronic properties were laboriously synthesized and investigated for potential applications in OSCs,[9,10] organic transistors (OTFTs),[11] and organic light-emitting diodes (OLEDs).[12,13] Most semiconductor polymers were constructed using aromatic heterocyclic monomers for their special electronic properties.[14,15] Among the various aromatic heteroring polymers, in general, an electron-rich aromatic monomer, or a polycyclic aromatic unit, is employed as the electron donating ingredient and an electron-deficient aromatic monomer functionalized with electron-withdrawing groups is used as the electron-accepting unit to prepare the so-called D−A (or push−pull) copolymers.[16] For electron-rich building blocks in the polymer field, carbazole (CBZ),[17,18] 5,11-dihydroindolo[3,2-*b*]carbazole (DCBZ),[19] and phenanthrocarbazole (PCBZ)[20−22] have been demonstrated to be the most versatile and effective building blocks for organic photoelectric materials. However, these three electron-rich donor blocks bind the same electron-lacking unit to construct a series of alternating copolymers, and their optoelectronic characteristics are still unknown. Especially, these donor blocks can greatly tune the energy level, the electron excitation and relaxation path, and the molecular packing behaviors. For bulk heterojunction solar cells, first, p-type and n-type materials strongly absorb light. The local dipole electron density is excited and redistributed to form a charge-separated (CS) state along the molecule.[23] Second, at the p−n domain interface, the CS state excitons overcome the Coulomb binding energy barrier and split to free charge.[24] The separation and recombination processes of electron−hole pair are very important for OSCs.[25,26] However, of particular importance is the single-molecule structure first excited by photons.[27,28] The molecular structure decides the electron excitation and separation pathway and efficiency.[29,30] Good understanding of this plays a crucial role in improving the efficiency of solar cells.[31−33] Here, the OSC performances of five polymers correlated to the ultrafast intramolecular charge splitting dynamics—namely, HXS-1 with CBZ polymerized at the 2 and 7 positions and 5,6-bis(octyloxy)benzo-2,1,3-thiadiazole (BOBT) at the 4 and 7 positions; HXS-2 and HXS-3 that

Received: August 4, 2019
Accepted: October 22, 2019
Published: November 4, 2019

DOI: 10.1021/acsomega.9b02476
ACS Omega 2019, 4, 19177−19182

contain PCBZ and BOBT, respectively; and HXS-4 and HXS-5 that coupled DCBZ with BOBT—were investigated.

RESULTS AND DISCUSSION

Structural and Optical Properties. The molecular structures of the five studied polymers are shown in Scheme 1 in the Experimental Section. The absorption spectra of

Scheme 1. Molecular Structures of Polymers Studied in This Work

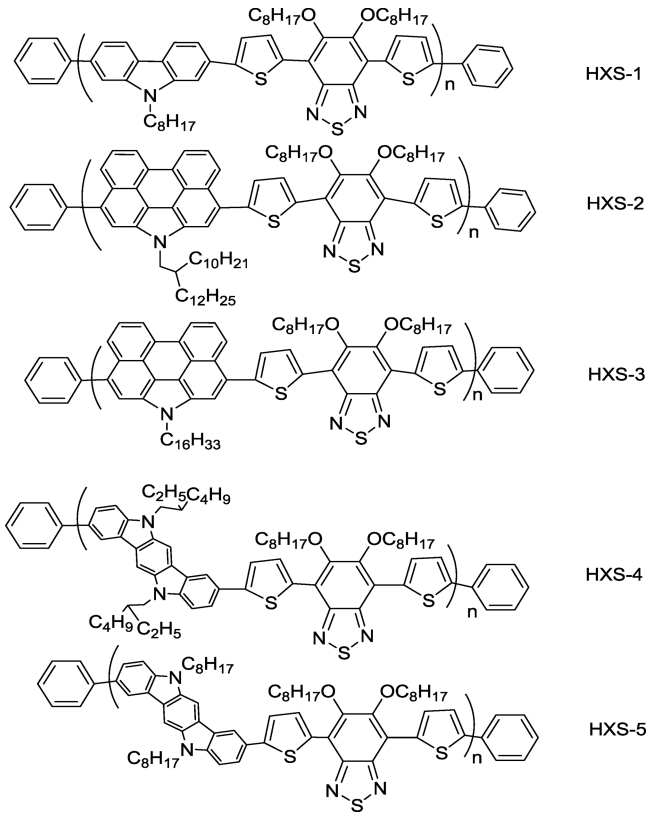

polymers HXS-1 to HXS-5 in chloroform solution and films are shown in Figure 1a,b. The key optical parameters and electrochemical results are summarized in Table 1. All polymers show two broad absorption bands in the range of 300−420 nm and 430−750 nm. Compared with HXS-1, the absorption peaks of HXS-2 and HXS-3) are broadened and blue-shifted both in solution and films. HXS-2 and HXS-3 show similar absorption spectra, which indicates that the alkyl

Table 1. Optical Properties of Copolymers

polymer	λ_{max} (film) (nm)	ε (M^{-1} cm^{-1})	band gap^{opt}	HOMO (eV)	LUMO (eV)
HXS-1	524	0.5×10^5	1.90	−5.22	−3.32
HXS-2	516	1.2×10^6	1.85	−5.15	−3.44
HXS-3	520	6.1×10^6	1.83	−5.22	−3.39
HXS-4	370	7.1×10^6	1.65	−5.32	−3.67
HXS-5	598	3.7×10^6	1.78	−5.08	−3.30

substituents on the PCBZ unit have a weak influence on the conjugation of the polymer main chain. However, the larger aromatic PCBZ in contrast to CBZ broadened the absorption range of the long-wavelength peak band by ∼20 nm. Carefully checking the spectra, HXS-2 bearing a branched alkyl on PCBZ exhibited a wider absorption band than HXS-3 bearing a linear alkyl. It was concluded that the intramolecular charge transfer (ICT) effect was disturbed by the flexible alkyl chain as a branch alkyl group facilitates electron conjugation along the aromatic main chain more effectively. This point was clearly supported by similar examples of HXS-4 and HXS-5. HXS-4 shows a strong and broadened absorption peak band between 400 and 750 nm. Compared with HXS-1 again, the absorption peak of HXS-4 in chloroform solution is markedly red-shifted due to the more electron-rich property of the DCBZ unit. By means of computational simulation, the torsion angles between carbazole architecture blocks and the acceptor are as follows: HXS-1 = 27.5°, HXS-2 = 64.5°, HXS-3 = 63.7°, HXS-4 = 1.6°, and HXS-5 = 1.3° (Figure S1). The calculation result is reasonable such that lower band gap polymers have smaller torsion angles. However, between the branched and linear alkyl group on the same donor blocks, the branched alkyl group facilitates electron delocalization along the conjugated backbone. Obviously, for HXS-4 and HXS-5, the experimental spectra data are mildly contradictory to the calculated torsion angles. This can be explained by the fact that the calculation did not consider the solvent effect but only the molecular configuration. Optical band gaps of HXS-1 to HXS-3 are almost at the same level (Table 1). Table 1 summarizes the optical properties and the highest occupied molecular orbital (HOMO) level. For the five polymers, HXS-4 gave the narrowest band gap of 1.65 eV (Figure S2).

Morphology. The active layer morphology greatly influences device performance.[34−38] X-ray diffraction (XRD) was employed to probe the polymer aggregation effect, as shown in Figure S3, for HXS-1, HXS-4, and HXS-5, it was clearly revealed that the polymers formed some degree of crystallinity and the $\pi-\pi$ distance between the main chains is

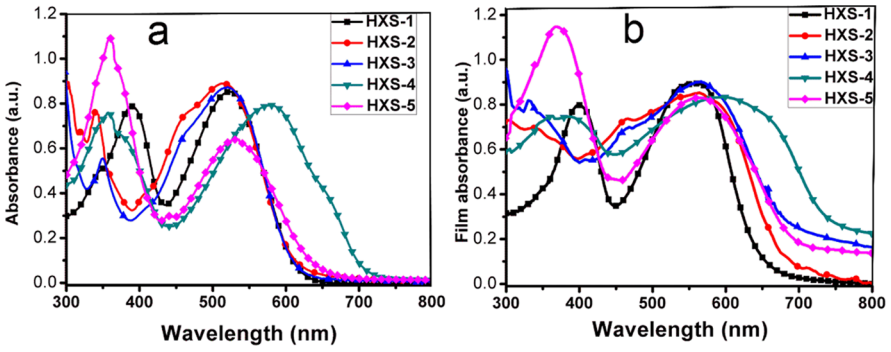

Figure 1. Ground-state absorption spectra of studied polymers (a) in dilute chloroform solution and (b) as a film.

DOI: 10.1021/acsomega.9b02476
ACS Omega 2019, 4, 19177−19182

Table 2. OSC Device Data and Polymer: $PC_{71}BM$ Blend Mobility

polymers	PCE% (average) maximum	V_{OC}	J_{SC}	FF	thickness (nm)	mobility (e) ($V/cm^2/s$)	mobility (h) ($V/cm^2/s$)
HXS-1	(5.83 ± 0.3) 6.3	0.86	9.69	0.69	85	7.00×10^{-5}	1.01×10^{-4}
HXS-2	(2.4 ± 0.1) 2.5	0.68	9.1	0.40	75	1.94×10^{-5}	1.61×10^{-5}
HXS-3	(2.5 ± 0.2) 2.7	0.68	9.79	0.42	70	2.09×10^{-5}	8.09×10^{-5}
HXS-4	(2.1 ± 0.2) 2.3	0.65	8.13	0.40	90	6.77×10^{-5}	4.37×10^{-6}
HXS-5	(0.7 ± 0.1) 0.8	0.63	3.34	0.38	95	3.07×10^{-4}	9.13×10^{-6}

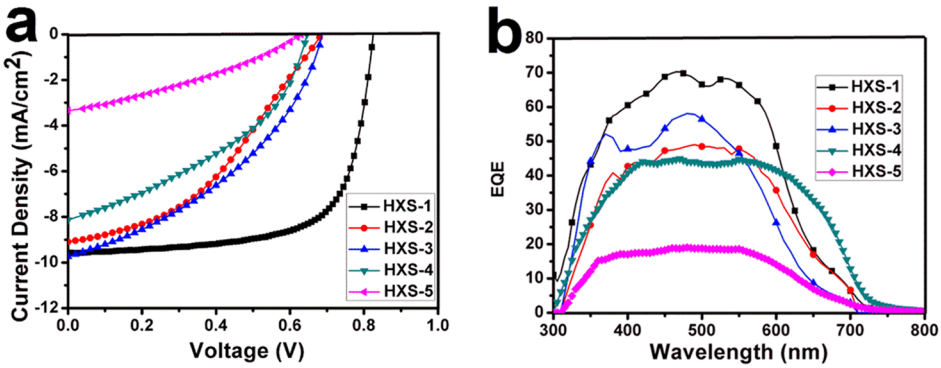

Figure 2. (a) $J-V$ curves of OSCs with 2.5% DIO (1,8-diiodooctane). (b) EQE curves of the OSCs.

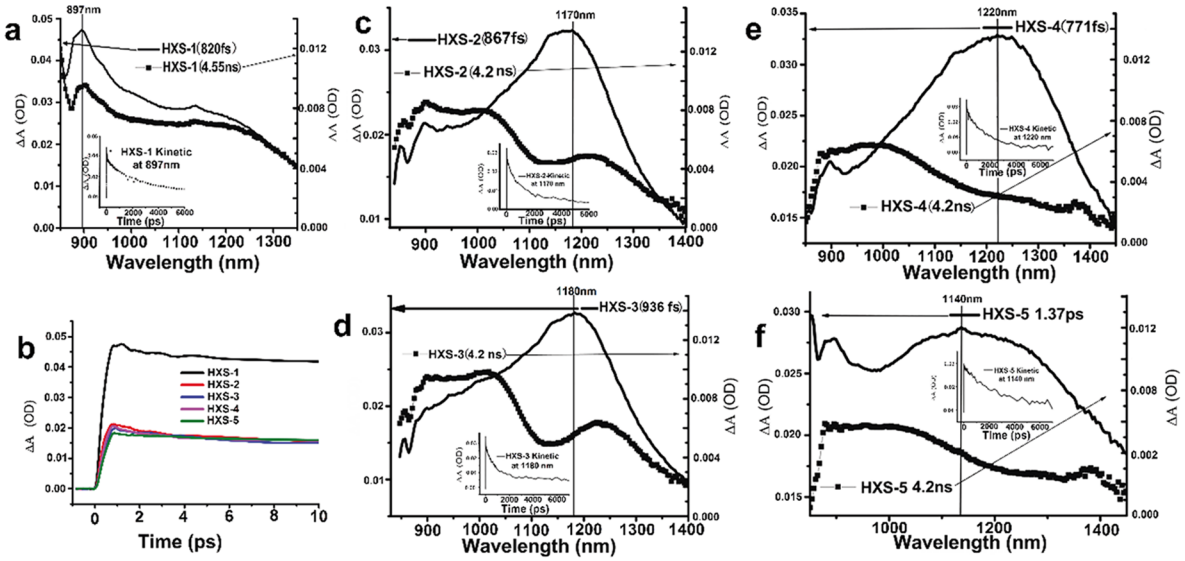

Figure 3. (a) Transient absorption spectra of HXS-1 at delay times of 820 fs and 4.55 ns. (b) Kinetic traces for all polymer transient spectroscopic features detected at 900 nm.; (c–f) Transient absorption spectra of HXS-2, HXS-3, HXS-4, and HXS-5 at delay times of 867 fs, 936, 771 fs, 1.37 ps, and 4.2 ns. The detection wavelengths are also correspondingly indicated.

0.39 nm for HXS-1, 0.40 nm for HXS-4, and 0.41 nm for HXS-5. A closer distance between polymer main chains, which are separated by the alkyl side chains are 1.07 nm for HXS-4 and 0.94 nm for HXS-5, compared with 1.7 nm of HXS-1. For the polymer with the bulky unit PCBZ, the crystallinity was destroyed and only a faint crystal trace can be perceived between 2θ = 30–50°. We surmised that this was caused by the large torsion angle, and the faint XRD signal comes from the large plane segment diffraction on the polymer main chain. Therefore, it can be concluded that polymers HXS-2 and HXS-3 are almost totally amorphous. The AFM and TEM images shown in Figure S4 provide direct evidence of the molecular chain interactions found in the polymers. HXS-1 obtained ideal phase separation with $PC_{71}BM$. The root mean square (RMS) value is 5.22 nm. For HXS-2, HXS-3, and HXS-4, these reference values are 1.23, 1.57, and 1.01 nm, respectively. For HXS-5, a big cluster was formed, and the RMS is 9.03 nm. The bottom TEM images (Figure S4) also disclosed this character. This in connection with the XRD analysis gave us some clues that bulky donor units and the affiliated alkyl side chain greatly changed the polymer aggregation ability and the consequent active layer morphology. Branched swallow-tail like alkyl (e.g. HXS-2 and HXS-4) facilitated a minor scale phase separation. The linear alky chains on HXS-3 and HXS-5 have the opposite effect such as a narrow absorption band and huge domain size. The weight-average molecular weights of these polymers are 51.4, 43.29, 46.62, 5.74, and 3.31 kg/mol for HXS-1 to HXS-5, respectively, and their corresponding polydispersity indices (PDIs) are 3.1, 1.93, 1.74, 1.52, and 1.21. Apart from HXS-1 obtaining a high molecular weight but wide PDI, the other polymers with a bulky donor unit had low molecular weights but narrow PDI. It revealed that the

DOI: 10.1021/acsomega.9b02476
ACS Omega 2019, 4, 19177–19182

molecular weights heavily depend on the donor block's solubility in the reaction mixture.

Device Performance. OSCs devices were fabricated to explore the photovoltaic performance of different polymers. Table 2 summarizes the photovoltaic parameters. The current density−voltage ($J-V$) plots and the external quantum efficiency (EQE) curves with the optimal photovoltaic performance under illumination of AM 1.5G (100 mW cm^{-2}) are shown in Figure 2. The device based on polymer HXS-1 has the best device data. Amorphous HXS-2 and HXS-3 provided poor fill factors for the reason of unideal phase separation. Moreover, the transient absorption (TA) spectra provide some strong evidence, which will be discussed later.

Figure S5 reveals that the exciton dissociation possibilities P_{diss} were 59.89 and 60.47% for HXS-2 and HXS-3, respectively, consequently leading to worse performances; meanwhile, this parameter is 72.5% for HXS-1. Benefiting from the broadened absorption band, HXS-4 showed a large short-circuit current density (J_{sc}) and a high PCE of 2.3% compared to HXS-5. The device P_{diss} of HXS-4 is 68.97%, which is also higher than the 57.3% of HXS-5. The EQE in Figure 2b also demonstrated this.

Ultrafast Spectra. TA spectra and dynamics after excitation with 450 nm pump light are shown in Figure 3. The TA spectra curves are broad across the 850−1400 nm region. For HXS-1, kinetic traces taken in the 897 nm region greatly decay within 0−2000 ps and do not show any change in spectral structure except intensity (inset in Figure 3a). The most striking absorption peak around 897 nm soon after excitation appeared and was assigned to the charge separate (CS) state. This assignment is because this signal located in the polymer cation steady-state absorption is featured in a spectrum band range that was obtained after adding an oxidant $FeCl_3$ into the solution (Figures S6 and S7). The high population of CS states and long life time cation decay characteristic (τ_1 = 2.62 ns) make it more easy to understand the high PCE result for HXS-1 (Figure 3b). The TA spectra and dynamics features for HXS-2 and HXS-3 reveal that a mixed absorption band including a small ratio of CS state population (830−1000 nm) (τ_1) and an intramolecular charge semi-separated (ICSS) state, which occupied a large ratio (1100−1400 nm) (τ_2) appeared soon after excitation (Figure 3c,d). The ICSS state is tentatively because the exciton had half-split into a hole−electron pair and is still close enough to undergo Coulombic attraction.[39] The short life time ICSS state decayed fast, which certainly does not produce any increase in the value of J_{sc} (Table S1). After approximately 4 ns, the long-lived CS state upthrust from the blend peak. Considering the molecular structure, it was unveiled that, to some extent, it is difficult to break the electron density symmetry in the excited state for large electron-donor-unit polymers (HXS-2 to HXS-5) to form CS state species. Consequently small proportions of the CS state for HXS-2 and HXS-3 are bound to a poor photovoltaic effect because only CS state carriers lastly become free charge.[40] HXS-4 and HXS-5 have similar features (Figure 3e,f) although HXS-2 and HXS-3 show longer CS state life times but a small population. However, carefully discerning Figure 3e,f, HXS-4 incipient excitation exhibited a narrow peak band (1100−1400 nm) compared to HXS-5, and this again supported the idea that branched alkyl groups facilitate electron delocalization along the conjugated backbone.

CONCLUSIONS

In summary, the photovoltaic efficiencies of five polymers furnished with different carbazole electron donor units were investigated. Apart from the universal facts relative to photovoltaic performance: materials light absorption spectra meet solar radiation and high absorption coefficient, energy level match, morphology ordering, charge mobility high and balance, we especially studied the singular molecular excitation, separation pathway, and efficiency that are the decisive factors of PCE. Large aromatic blocks have a broad electron delocalization domain; thus, it is difficult to break the excited state electron density symmetry to form large populations of CS-state species. This key fact greatly deteriorates the device photovoltaic performance.

EXPERIMENTAL SECTION

All the polymers are diagrammed in Scheme 1.

HXS-1, HXS-4, and HXS-5 were prepared according to the literature,[4,32] and their characterizations are given in the Supporting Information (Figures S9−15). Details of the synthesis of HXS-2 and HXS-3) and the necessary intermediates are described in the Supporting Information (Schemes S1 and S2).

ASSOCIATED CONTENT

Supporting Information

The Supporting Information is available free of charge on the ACS Publications website at DOI: 10.1021/acsomega.9b02476.

Experiment details, polymer synthesis, NMR, XRD, AFM, TEM, CV, torsion angle calculation, and kinetic traces for all polymers transient spectroscopic features detected at 1200 nm (PDF)

AUTHOR INFORMATION

Corresponding Authors

*E-mail: qinruiping@163.com (R.Q.).
*E-mail: qinch@hotmail.com (C.Q.).

ORCID

Ruiping Qin: 0000-0002-1920-8704
Yurong Jiang: 0000-0001-8022-3965
Zhiyong Liu: 0000-0003-1584-8162

Notes

The authors declare no competing financial interest.

ACKNOWLEDGMENTS

The authors thank the China Scholarship Council Scholarship fund (CSC201508410221), National Natural Science Foundation Project of China (grant no. 11804084), the Advanced Technology Research Program of Henan Province (grant no. 182102210369), and the Foundation for Key Program of Education Department of Henan Province (grant nos. 19A140011 and 20A140017). The authors thank Professor Jishan Wu (NUS) for the help in the experiments (compound **6** was synthesized by Wu's group in Singapore by R.Q.).

REFERENCES

(1) Hong, J.; Wang, C.; Cha, H.; Kim, H. N.; Kim, Y.; Park, C. E.; An, T. K.; Kwon, S.-K.; Kim, Y.-H. Morphology driven by molecular structure of thiazole-based polymers for use in field-effect transistors and solar cells. *Chem. − Eur. J.* **2019**, *25*, 649−656.

DOI: 10.1021/acsomega.9b02476
ACS Omega 2019, 4, 19177−19182

(2) Cui, Y.; Yao, H.; Zhang, J.; Zhang, T.; Wang, Y.; Hong, L.; Xian, K.; Xu, B.; Zhang, S.; Peng, J.; Wei, Z.; Gao, F.; Hou, J. Over 16% efficiency organic photovoltaic cells enabled by a chlorinated acceptor with increased open-circuit voltages. *Nat. Commun.* **2019**, *10*, 2515.
(3) Chu, S.; Majumdar, A. Opportunities and challenges for a sustainable energy future. *Nature* **2012**, *488*, 294.
(4) Qin, R.; Li, W.; Li, C.; Du, C.; Veit, C.; Schleiermacher, H.-F.; Andersson, M.; Bo, Z.; Liu, Z.; Inganäs, O.; Wuerfel, U.; Zhang, F. A planar copolymer for high efficiency polymer solar cells. *J. Am. Chem. Soc.* **2009**, *131*, 14612−14613.
(5) Balar, N.; Rech, J. J.; Henry, R.; Ye, L.; Ade, H.; You, W.; O'Connor, B. T. The importance of entanglements in optimizing the mechanical and electrical performance of all-polymer solar cells. *Chem. Mater.* **2019**, *31*, 5124.
(6) Xu, X.; Feng, K.; Bi, Z.; Ma, W.; Zhang, G.; Peng, Q. Single-junction polymer solar cells with 16.35% efficiency enabled by a platinum(ii) complexation strategy. *Adv. Mater.* **2019**, *31*, 1901872.
(7) Yuan, J.; Zhang, Y.; Zhou, L.; Zhang, G.; Yip, H.-L.; Lau, T.-K.; Lu, X.; Zhu, C.; Peng, H.; Johnson, P. A.; Leclerc, M.; Cao, Y.; Ulanski, J.; Li, Y.; Zou, Y. Single-junction organic solar cell with over 15% efficiency using fused-ring acceptor with electron-deficient core. *Joule* **2019**, *3*, 1140−1151.
(8) Kan, B.; Feng, H.; Yao, H.; Chang, M.; Wan, X.; Li, C.; Hou, J.; Chen, Y. A chlorinated low-bandgap small-molecule acceptor for organic solar cells with 14.1% efficiency and low energy loss. *Sci. China: Chem.* **2018**, *61*, 1307.
(9) Qin, R.; Guo, D.; Li, M.; Li, G.; Bo, Z.; Wu, J. Perylene monoimide dimers enhance ternary organic solar cells efficiency by induced d−a crystallinity. *ACS Appl. Energy Mater.* **2019**, *2*, 305−311.
(10) Balar, N.; Xiong, Y.; Ye, L.; Li, S.; Nevola, D.; Dougherty, D. B.; Hou, J.; Ade, H.; O'Connor, B. T. Role of Polymer Segregation on the Mechanical Behavior of All-Polymer Solar Cell Active Layers. *ACS Appl. Mater. Interfaces* **2017**, *9*, 43886−43892.
(11) Fu, B.; Wang, C.; Sun, Y.; Yao, J.; Wang, Y.; Ge, F.; Yang, F.; Liu, Z.; Dang, Y.; Zhang, X.; Shao, X.; Li, R.; Hu, W. A "phase separation" molecular design strategy towards large-area 2d molecular crystals. *Adv. Mater.* **2019**, *31*, 1901437.
(12) Byeon, S. Y.; Lee, D. R.; Yook, K. S.; Lee, J. Y. Recent progress of singlet-exciton-harvesting fluorescent organic light-emitting diodes by energy transfer processes. *Adv. Mater.* **2019**, *31*, 1803714.
(13) May, F.; Al-Helwi, M.; Baumeier, B.; Kowalsky, W.; Fuchs, E.; Lennartz, C.; Andrienko, D. Design rules for charge-transport efficient host materials for phosphorescent organic light-emitting diodes. *J. Am. Chem. Soc.* **2012**, *134*, 13818−13822.
(14) Huang, H.; Guo, Q.; Feng, S.; Zhang, C.; Bi, Z.; Xue, W.; Yang, J.; Song, J.; Li, C.; Xu, X.; Tang, Z.; Ma, W.; Bo, Z. Noncovalently fused-ring electron acceptors with near-infrared absorption for high-performance organic solar cells. *Nat. Commun.* **2019**, *10*, 3038.
(15) Zhu, J.; Liu, Q.; Li, D.; Xiao, Z.; Chen, Y.; Hua, Y.; Yang, S.; Ding, L. A Wide-Band Gap Copolymer Donor for Efficient Fullerene-Free Solar Cells. *ACS Omega* **2019**, 14800.
(16) Qin, R.; Yang, J.; Li, P.; Wu, Q.; Zhou, Y.; Luo, H.; Chang, F. Structure property relationship for carbazole and benzothiadiazole based conjugated polymers. *Sol. Energy Mater. Sol. Cells* **2016**, *145*, 412−417.
(17) Qin, R.; Bo, Z. Synthesis and characterization of 2,7-linked carbazole oligomers. *Macromol. Rapid Commun.* **2012**, *33*, 87−91.
(18) Qin, R.; Jiang, Y.; Ma, H.; Yang, L.; Liu, H.; Chang, F. Carbazoles on same main chain for polymer solar cells. *J. Appl. Polym. Sci.* **2013**, *129*, 2671−2678.
(19) Sharma, B.; Sarothia, Y.; Singh, R.; Kan, Z.; Keivanidis, P. E.; Jacob, J. Synthesis and characterization of light-absorbing cyclopentadithiophene-based donor−acceptor copolymers. *Polym. Int.* **2016**, *65*, 57−65.
(20) Yang, L.; Yao, Z.; Liu, J.; Wang, J.; Wang, P. A systematic study on the influence of electron-acceptors in phenanthrocarbazole dye-sensitized solar cells. *ACS Appl. Mater. Interfaces* **2016**, *8*, 9839−9848.
(21) Chen, H.; Guo, Y.; Sun, X.; Gao, D.; Liu, Y.; Yu, G. Synthesis and characterization of phenanthrocarbazole−diketopyrrolopyrrole copolymer for high-performance field-effect transistors. *J. Polym. Sci., Part A: Polym. Chem.* **2013**, *51*, 2208−2215.
(22) Sung, M. J.; Yoon, S.; Kwon, S.-K.; Kim, Y.-H.; Chung, D. S. Synthesis of phenanthro[1,10,9,8-cdefg]carbazole-based conjugated polymers for green-selective organic photodiodes. *ACS Appl. Mater. Interfaces* **2016**, *8*, 31172−31178.
(23) Rolczynski, B. S.; Szarko, J. M.; Son, H. J.; Liang, Y.; Yu, L.; Chen, L. X. Ultrafast intramolecular exciton splitting dynamics in isolated low-band-gap polymers and their implications in photovoltaic materials design. *J. Am. Chem. Soc.* **2012**, *134*, 4142−4152.
(24) Guo, Z.; Lee, D.; Schaller, R. D.; Zuo, X.; Lee, B.; Luo, T.; Gao, H.; Huang, L. Relationship between interchain interaction, exciton delocalization, and charge separation in low-bandgap copolymer blends. *J. Am. Chem. Soc.* **2014**, *136*, 10024−10032.
(25) Zhan, X.; Li, Y. A new perspective for organic solar cells: triplet nonfullerene acceptors. *Sci. China: Chem.* **2018**, *61*, 637.
(26) Alamoudi, M. A.; Khan, J. I.; Firdaus, Y.; Wang, K.; Andrienko, D.; Beaujuge, P. M.; Laquai, F. Impact of nonfullerene acceptor core structure on the photophysics and efficiency of polymer solar cells. *ACS Energy Lett.* **2018**, *3*, 802−811.
(27) Balawi, A. H.; Stappert, S.; Gorenflot, J.; Li, C.; Müllen, K.; Andrienko, D.; Laquai, F. Direct and energy-transfer-mediated charge-transfer state formation and recombination in triangulene-spacer-perylenediimide multichromophores: lessons for photovoltaic applications. *J. Phys. Chem. C* **2019**, *123*, 16602−16613.
(28) Goyal, P.; Hammes-Schiffer, S. Tuning the ultrafast dynamics of photoinduced proton-coupled electron transfer in energy conversion processes. *ACS Energy Lett.* **2017**, *2*, 512−519.
(29) Hörmann, U.; Zeiske, S.; Piersimoni, F.; Hoffmann, L.; Schlesinger, R.; Koch, N.; Riedl, T.; Andrienko, D.; Neher, D. Stark effect of hybrid charge transfer states at planar ZnO/organic interfaces. *Phys. Rev. B* **2018**, *98*, 155312.
(30) Niladari Raju, M. V.; Mohanty, M. E.; Bangal, P. R.; Vaidya, J. R. Synthesis and ultrafast dynamics of a donor−acceptor−donor molecule having optoelectronic properties. *J. Phys. Chem. C* **2015**, *119*, 8563−8575.
(31) Poelking, C.; Andrienko, D. Design rules for organic donor−acceptor heterojunctions: pathway for charge splitting and detrapping. *J. Am. Chem. Soc.* **2015**, *137*, 6320−6326.
(32) Liu, Y.; Zuo, L.; Shi, X.; Jen, A. K. Y.; Ginger, D. S. Unexpectedly slow yet efficient picosecond to nanosecond photo-induced hole-transfer occurs in a polymer/nonfullerene acceptor organic photovoltaic blend. *ACS Energy Lett.* **2018**, *3*, 2396−2403.
(33) Qin, R.-P.; Song, G.-L.; Jiang, Y.-R.; Bo, Z.-S. Planar donor-acceptor copolymers for bulk heterojunction solar cells. *Chem. J. Chinese U.* **2012**, *33*, 828−832.
(34) Li, W.; Zhou, Y.; Viktor Andersson, B.; Mattias Andersson, L.; Thomann, Y.; Veit, C.; Tvingstedt, K.; Qin, R.; Bo, Z.; Inganäs, O.; Würfel, U.; Zhang, F. The effect of additive on performance and shelf-stability of HSX-1/PCBM photovoltaic devices. *Org. Electron.* **2011**, *12*, 1544−1551.
(35) Ye, L.; Jiao, X.; Zhang, S.; Yao, H.; Qin, Y.; Ade, H.; Hou, J. Control of mesoscale morphology and photovoltaic performance in diketopyrrolopyrrole-based small band gap terpolymers. *Adv. Energy Mater.* **2017**, *7*, 1601138.
(36) Ye, L.; Hu, H.; Ghasemi, M.; Wang, T.; Collins, B. A.; Kim, J.-H.; Jiang, K.; Carpenter, J. H.; Li, H.; Li, Z.; McAfee, T.; Zhao, J.; Chen, X.; Lai, J. L. Y.; Ma, T.; Bredas, J.-L.; Yan, H.; Ade, H. Quantitative relations between interaction parameter, miscibility and function in organic solar cells. *Nat. Mater.* **2018**, *17*, 253−260.
(37) Ye, L.; Zhao, W.; Li, S.; Mukherjee, S.; Carpenter, J. H.; Awartani, O.; Jiao, X.; Hou, J.; Ade, H. High-efficiency nonfullerene organic solar cells: critical factors that affect complex multi-length scale morphology and device performance. *Adv. Energy Mater.* **2017**, *7*, 1602000.
(38) Lu, X. F.; Chen, Y.; Wang, S.; Gao, S.; Lou, X. W. Interfacing Manganese Oxide and Cobalt in Porous Graphitic Carbon Polyhedrons Boosts Oxygen Electrocatalysis for Zn−Air Batteries. *Adv. Mater.* **2019**, *31*, 1902339.

DOI: 10.1021/acsomega.9b02476
ACS Omega 2019, 4, 19177−19182

(39) Westerling, M.; Aarnio, H.; Österbacka, R.; Stubb, H.; King, S. M.; Monkman, A. P.; Andersson, M. R.; Jespersen, K.; Kesti, T.; Yartsev, A.; Sundström, V. Photoexcitation dynamics in an alternating polyfluorene copolymer. *Phys. Rev. B* **2007**, *75*, 224306.
(40) Wang, X.; Kan, B.; Kuang, Z.; Song, H.; Long, G.; Guo, Q.; Chen, Y.; Xia, A. Unveiling the molecular symmetry dependence of exciton dissociation processes in small-molecular heterojunctions. *J. Phys. Chem. C* **2018**, *122*, 26851−26856.

DOI: 10.1021/acsomega.9b02476
ACS Omega 2019, 4, 19177−19182